Fast Infrared Small Target Detection Based on Global Contrast Measure Using Dilate Operation

Ye Tang, Kun Xiong, and Chunxi Wang

Abstract— **Infrared small target images are not conducive to detection due to their low visibility. Although there are many algorithms have been proposed to solve this problem, existing methods inevitably struggle to strike a good balance between efficiency and performance. This letter proposes a fast infrared small target detection algorithm with a low computational time consumption, only 0.012 s, while maintaining excellent detection performance. There are only two steps in the proposed method. First, the original image is processed by dilate operation with a ring structuring element. Then, the final detection result is calculated by global contrast measure (GCM) between the original image and the processed image according to the ratio form and the difference form. The experimental results demonstrate that the proposed method consistently achieves a robust and effective performance on six real sequences. In particular, the speed of the proposed method is at least two times faster than the state-of-the-art methods.**

Index Terms— **Dilate operation, fast, global contrast measure (GCM), infrared image, low computational time consumption.**

I. Introduction

INFRARED small target detection is one of the key technologies in infrared search and track (IRST). It has a wide range of applications in prewarning, precise guidance, and maritime surveillance. However, the following difficulties in IRST detection await improvement: infrared small targets are easily drowned by complicit backgrounds due to the presence of serious noise and clutter; infrared small target detection, generally, is a standoff imaging, which gives rise to small targets without shape and texture information to exploit [1]. To improve the accuracy and real-time performance of infrared small target detection, mounting infrared small target detection algorithms have been proposed.

Traditional methods such as TopHat filter [2] and MaxMean filter [3] methods attempt to suppress the image background and detect targets in accordance with the structural prior knowledge of the target. However, they are sensitive to intensity edge and structural background clutter. Gao et al. [4] proposed a matrix factorization-based infrared small-target detection algorithms by using local patch construction. Zhang and Peng [5], on the basis of the infrared patch-tensor (IPT) model, proposed a novel nonconvex low-rank constraint named partial sum of tensor nuclear norm (PSTNN) joint weighted l_1 norm that was employed to efficiently suppress the background and enhance the target. Although these algorithms are convergently guaranteed, most of them are inefficient due to full singular value decomposition (SVD) operation. Aghaziyarati et al. [6] used the average absolute gray difference (AAGD) algorithm to suppress background noise by using local averaging and enhancing the target area by adopting local contrast. Moradi et al. [7] further laid out a directional approach called the absolute directional mean difference (ADMD) algorithm. Moreover, directional information is adopted in most of them to suppress complex background edges better. However, they use absolute local contrast without eliminating high-brightness backgrounds effectively. Zhang et al. [8] calculated the local intensity and gradient (LIG) map from the original infrared image to enhance the targets and suppress clutters. Furthermore, Kwan et al. [9] consist of a video resolution enhancement module with LIG. Wang et al. [10] fuse the local-scale, blob-based contrast map, and gradient map in the detection stage. Chen et al. [11] extract the targets via iterative segmentation. However, it is a pity that these filters failed to handle complex scenes full of edges and interferences well.

In recent years, some local contrast and human visual system (HVS)-based methods have been introduced to the infrared small target detection field, such as the methods based on local contrast measure (LCM) [12] and multiscale patch-based contrast measure (MPCM) [13]. Similarly, these methods are susceptible to highlighting noise and introducing false targets during the operation, which increases the false alarm rate. Following further analysis, due to the point spread function of the optical system, light waves converge and interfere at the focal point, which produces a diffraction pattern of concentric rings surrounding a central bright disk, and background edges usually distribute along a specific direction [14]. Consequently, some researchers tried to further suppress background via more structural information usage around the target. Wu et al. [15] proposed the double-neighborhood gradient method (DNGM). Nie et al. [16] considered the local homogeneity. Shi et al. [17] proposed a high-boost-based multiscale LCM (HBMLCM) in which a high-boost (HB) filter was used to enhance the high-frequency component while retaining the low-frequency one. Han et al. [18] recommended multiscale trilayer LCM (TLLCM) to enhance the true target purposefully in line with the target shape. Meanwhile, many joint algorithms had been proposed. Pan et al. [19] utilized the difference between the target and the outer neighborhood

Manuscript received 31 October 2022; revised 22 December 2022; accepted 30 December 2022. Date of publication 3 January 2023; date of current version 2 February 2023. *(Corresponding author: Chunxi Wang.)*

The authors are with the Beijing Aerospace Institute for Metrology and Measurement Technology, China Academy of Launch Vehicle Technology, Beijing 100076, China (e-mail: tangye111@163.com; chunxiww@163.com).

Digital Object Identifier 10.1109/LGRS.2023.3233958

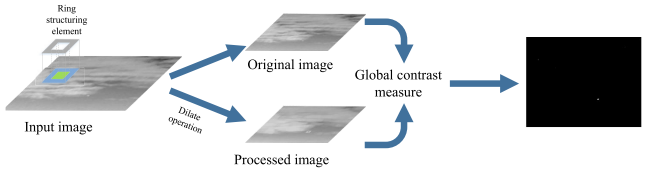

Fig. 1. Flowchart of the proposed method.

as the weighted function. Cui et al. [20] fused local contrast with compressed sensing. Han et al. [21] incorporated local contrast with adaptive background estimation. Xia et al. [22] put forward a new dissimilarity degree called the local energy factor (LEF) to measure the brightness difference between the small targets and the backgrounds. However, these methods use more image information to have a good detection effect, but they are not workable for real-time applications owing to high computational complexity.

To enhance and detect infrared dim small targets embedded in clutter background simply and efficiently, in this letter, a novel algorithm based on global contrast measure (GCM) using the dilation method is proposed. It is derived from LCM. However, this method used a sliding nine-rectangle-grid window to enhance the target and suppress the background, which calculated the local contrast value eight times, giving rise to poor real-time performance. To this end, a new ring structure suggested by Bai et al. [23] shows excellent performance in the new TopHat transformation, inspiring our fast detection model. The dilate operation replaces the gray value of the center of the ring structuring element with the maximum gray value of the ring background, which widened the contrast between the gray values of the original image and the processed image in the target region. To be concise, only two steps are contained in our method: there are dilation method and GCM (ratio form and difference form). Particularly, the proposed method has extremely low computational time consumption.

The remainder of this letter is organized as follows. In Section II, our fast detection method is introduced in detail. In Section III, experimental results carried on a set of real infrared images covering typical backgrounds with buildings, sky, and various clutters are shown. Conclusion is delivered in Section IV.

II. Proposed Method

The flowchart of the proposed method is shown in Fig. 1. First, the input image is processed by dilate operation which uses the ring structure. Furthermore, GCM is used to enhance the real target and suppress background clutter.

A. Global Contrast Measure

The mathematical morphology operation: dilation, which works with two sets, one set is the original image, and the other one is the ring structuring element. Let f and ΔB represent the original image and ring structuring element, respectively. The dilation of f by ΔB, denoted by $f \oplus \Delta B$. The image after dilate operation is defined as

$$I_d = f \oplus \Delta B. \tag{1}$$

The local contrast value will be calculated between the target region and the surrounding region. There are many definitions of local contrast in recent years, which can be roughly divided into the ratio form and the difference form. The ratio-form local contrast is used to enhance the true target, and the difference-form local contrast can suppress the clutter background. In this letter, both the ratio form and difference form are used to calculate the global contrast value, and for each pixel, its GCM is defined as

$$\mathrm{GCM} = \left(\frac{I_{\mathrm{ori}}}{I_d} I_{\mathrm{ori}} - I_{\mathrm{ori}}\right) \tag{2}$$

where I_{ori} means the original image.

$f \oplus \Delta B$ uses the margin region of the ring structuring element to fulfill dilate operation, which means $f \oplus \Delta B$ uses the maximum pixel of surrounding regions to replace the pixel of the central region. However, if the processed region is not a target region, the relationship of the gray value of the pixels between the processed region and the surrounding region is not confirmed, which causes the uncertainty between I_{ori}^2/I_d and I_{ori}. This property indicates that there may be negative values in GCM. To avoid this situation, GCM can be modified as

$$\begin{aligned} \mathrm{GCM} &= \max\left(\frac{I_{\mathrm{ori}}}{I_d} I_{\mathrm{ori}} - I_{\mathrm{ori}}, 0\right) \\ &= \max\left(\frac{I_{\mathrm{ori}}}{I_d} I_{\mathrm{ori}} - I_{\mathrm{ori}}, I_{\mathrm{ori}} - I_{\mathrm{ori}}\right) \\ &= \max\left(\frac{I_{\mathrm{ori}}}{I_d} I_{\mathrm{ori}}, I_{\mathrm{ori}}\right) - I_{\mathrm{ori}}. \end{aligned} \tag{3}$$

Let $\mathrm{NC}_{od} = \max(I_{\mathrm{ori}}^2/I_d, I_{\mathrm{ori}})$, then the modified GCM can be defined as follows:

$$\mathrm{GCM} = (\mathrm{NC}_{od} - I_{\mathrm{ori}}) \tag{4}$$

where the nonnegative constraint is used to eliminate clutter further since the true target region in the original image is brighter than its corresponding region in the processed image.

Algorithm 1 Proposed Small Target Detection Method Based on the GCM

Input: Original Image
Output: GCM map.
1: Obtain the image through dilate operation.
2: Compute GCM according to Eq. (4)
3: **return** GCM map.

B. Detection Ability Analysis

It gets clear from the definition that GCM can enhance the target and suppress the background. The definition of dilation indicates that dilation is the operation of finding the local maximum in the scope of the structuring element, and this property gives rise to the replacement from the gray value of the center to the maximum gray value of the surrounding area. If the current location is the target region in the original image, after dilate operation, the surrounding region will be bright and the target region will be dim in the processed image. Consequently, the gray value of the target region in the original image is much larger than the corresponding region in the processed image. It can be easily drawn from the ratio form that the target can be enhanced. Conversely, if the current

location is the background in the original image, the gray value of the background region in the original image is similar to the corresponding region in the processed image. It can be easily drawn from the difference form that the background can be suppressed.

The GCM of the pixel belonging to the target is given by

$$\mathrm{GCM}^t = \frac{I^t_{\mathrm{ori}}}{I^t_d} I^t_{\mathrm{ori}} - I^t_{\mathrm{ori}} \tag{5}$$

where I^t_{ori} is the target region in the original image. I^t_d is the corresponding target region in the processed image. It is easy to find that

$$\frac{I^t_{\mathrm{ori}}}{I^t_d} > 1. \tag{6}$$

The target in the original image is much brighter than the corresponding pixel in the processed image. The GCM of the pixel belonging to the background is given by

$$\mathrm{GCM}^b = \frac{I^b_{\mathrm{ori}}}{I^b_d} I^b_{\mathrm{ori}} - I^b_{\mathrm{ori}} \tag{7}$$

where I^b_{ori} is the background region in the original image. I^b_d is the corresponding background region in the processed image. For the most part, we have

$$\frac{I^b_{\mathrm{ori}}}{I^b_d} \leq 1. \tag{8}$$

The GCM in the target region is much higher than that in the background region. Consequently, the GCM map can be used to detect the target. This reveals that the proposed method ponders the situation of target enhancement and background elimination simultaneously.

C. Relationship Between the Proposed Method and LCM

The proposed method and LCM model both utilize the HVS to process the image information. However, there are some differences between the two algorithms. The differences are summarized as follows.

1) The LCM needs to calculate the contrast value in eight directions, accordingly, the LCM repeats the calculation eight times. Whereas the proposed method ingeniously utilizes dilate operation to obtain the contrast in one step only.

2) The LCM essentially highlights the target by widening the contrast between the target and the background, which failed to suppress the background completely. While the proposed method utilizes the difference form to carry out a thorough elimination of the background.

3) The LCM carries out the pooling operation over different scales, this operation may change the morphology of small target [12]. Conversely, the introduction of the morphological method (dilate operation) will preserve the morphology of small targets intact [24].

III. Experimental Results and Analysis

In this section, the datasets, the baseline comparison methods, and the evaluation metrics are introduced first. Then, qualitative and quantitative results are offered to demonstrate the performance of all methods.

TABLE I
Details of Six Infrared Target Datasets Used in the Experiments

Seq	Frame	Image Resolution	Target Size	Target Shape
1	324	256×256, 512×640	3×3 to 8×8	Rectangular
2	264	256×256, 512×640	3×3 to 6×6	Circular
3	276	256×256, 512×640	3×3 to 6×6	Circular
4	213	512×640	3×3	Circular
5	242	512×640	3×3	Circular
6	247	512×640	3×3	Circular

A. Datasets, Baseline Methods, and Evaluation Metrics

1) Datasets: The dataset in experiments contains six actual infrared image sequences [8], [25], [26], [27], including clutter backgrounds such as cloudy sky, sea, architecture, and mountain. The details about targets are described in Table I.

2) Baseline Methods: Our proposed method is compared with ten baseline methods, including two conventional methods (TopHat filter [2] and MaxMean filter [3]), two directional information-based methods (ADMD [7] and AAGD [6]), three multiscale LCM-based methods (LCM [12], HBLCM [17], and TLLCM [18]), local patch construction decomposition-based method (PSTNN [5]), and LIG properties-based method (LIG [8]).

3) Evaluation Metrics: There are three commonly used metrics, including receiver-operating characteristic curve (ROC), signal-to-clutter ratio gain (SCRG), and background suppression factor (BSF), which are used to evaluate the performance of infrared small target detection algorithms.

B. Qualitative Results

Target detection results processed by different baseline methods on the six sequences are illustrated in Fig. 2. A random image from each sequence is selected to demonstrate the filtering results. For better visualization, the target area is enlarged, and a close-up version is displayed in the left-bottom part. In the comparison with the baseline methods, GCM achieves better performance on target enhancement and background suppression for all sequences.

Three representative filtering results of sequences 1–3 are shown in Fig. 2. The two conventional filtering methods (TopHat, MaxMean) can enhance the target to a certain extent, but they are inferior to the other methods in background suppression. Nevertheless, the AAGD, ADMD, and HBLCM methods only preserve the shape of the target, conversely, the brightness of the target has become dimmer, and both methods perform poorly in three images. The LCM method has been demonstrated to effectively enhance the target in sequence 3, while its robustness in detecting the target in sequences 1 and 3 is limited, as the enhancement of the target is not readily apparent. The TLLCM method can achieve good target enhancement and background suppression results in sequence 2. However, TLLCM is not robust enough to detect the target in sequences 1 and 3, and the enhancement is not evident. In terms of target enhancement, the LIG and PSTNN methods perform better, but they are also sensitive to strong building edges and horizontal sky-building clutters. In general, the detection results processed by the baseline methods on three images demonstrate that the clusters of river–land edge,

TABLE II

AVERAGE SCRG VALUES, BSF VALUES, AND TIME COSTS OBTAINED ON THE THREE CONSIDERED DATASETS BY DIFFERENT METHODS. THE FIRST TWO BEST RESULTS FOR EACH ROW ARE REPORTED IN ITALIC BOLD AND UNDERLINED, RESPECTIVELY

Methods		TopHat	MaxMean	ADMD	AAGD	HBLCM	TLLCM	LCM	PSTNN	LIG	Proposed
SCRG	Seq1	11.25	10.91	14.19	71.27	24.73	49.38	23.54	136.1	***293.11***	205.28
	Seq2	8.68	7.66	38.26	70.66	29.96	78.05	18.56	47.12	75.9	***146.81***
	Seq3	23.74	23.13	32.6	391.34	36.81	109.36	40.61	229.86	***812.25***	757.8
	Seq4	6.2	6.59	10.71	9.35	6.59	36.9	8.56	40.31	24.11	***105.74***
	Seq5	7.81	8.51	23.45	37.64	10.81	83.19	15.62	45.46	54.19	***162.18***
	Seq6	8.69	8.58	16.7	27.35	37.22	47.19	34.78	69.77	152.15	***201.28***
BSF ($\times 10^3$)	Seq1	4.06	4.91	7.38	0.16	0.13	30.41	0.53	***57.03***	0.29	31.51
	Seq2	2.82	3.66	1.55	0.15	0.04	1.38	0.86	10.36	5.45	***13.57***
	Seq3	4.28	4.88	4.65	0.26	0.16	43.68	2.28	43.82	6.97	***43.87***
	Seq4	1.27	1.62	0.93	0.06	0.01	6.72	0.96	8.06	0.74	***10.93***
	Seq5	1.58	2.2	0.79	0.06	0.02	3.83	0.85	***11.46***	1.5	9.4
	Seq6	1.99	2.59	0.78	0.08	0.04	8.08	1.86	***16.97***	3.35	10.78
Time (s)	640×512	0.022	0.041	0.032	0.132	0.064	13.112	0.235	1.024	5.325	***0.012***

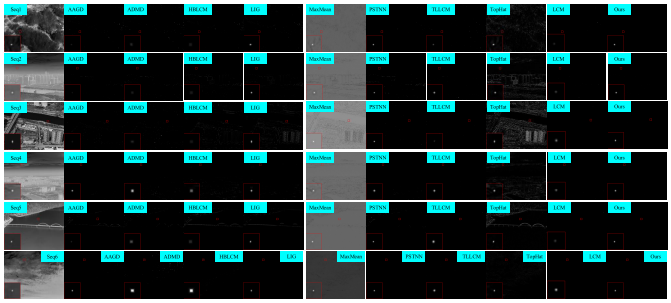

Fig. 2. (Top to bottom) Detection result of sequences 1–6 using the proposed algorithm.

building edge, and plant edge cause false alarms, whereas these clusters are well suppressed by the proposed method.

For sequences 4–6. The result describes that TopHat and MaxMean methods have a lot of clutter interference. The AAGD, ADMD, and HBLCM methods perform better on target enhancement in sequences 4 and 6. However, AAGD fails to detect the target for sequence 5. The enhancement of the target in sequence 5 of LCM is not evident. The TLLCM method achieves satisfactory results, and there is little noise in the background. The LIG and PSTNN methods achieve good performance in target detection and background suppression. But LIG still has residual noise in sequence 5, and it is sensitive to the bridge edge.

Consequently, the experimental results prove that our method enjoys the better capability of target enhancement and background suppression than other baseline methods, meanwhile, working robustly in a complex background.

C. Quantitative Results

The detection performances of the proposed method and the other baseline methods are further evaluated by using SCRG, BSF, and ROC curves on six sequences.

The average SCRG and BSF results obtained by our method and the baseline methods are summarized in Table II. It is observed that our method obtains the highest scores in terms of SCRG on sequences 2 and 4–6, while our method also achieved the second highest score on sequences 1 and 3. Meanwhile, facing the varying characteristic of these sequences, our method enjoys the better capability of background suppression. In the comparison with the baseline method, the BSF value of our method is higher than that of the baseline method. Only on sequences 1, 5, and 6, our method is inferior to PSTNN.

The characteristic of the ROC curve is a graphical plot of the detection probabilities versus the false alarm rates. The ROC curves were obtained by the different methods for the six real sequences in Fig. 3. It can be seen that the ROC curves achieved by our method on the six sequences are closer to the upper left corner than other baseline methods, which means that our method has the best performance in terms of both FPR and TPR. In addition, the area under the curve AUC of each method is calculated. AUC is widely utilized to access the classification performance of true or false targets. The AUC value is in the range of 0–1, as shown in Fig. 3. The larger AUC value means better target detection performance in the ROC curve evaluation system. Consequently, our method achieves the best performance on the six sequences, which is to say that our method has the excellent capability of robustness against various intricate backgrounds.

D. Complexity Analysis and Computational Time Consumption Comparison

Finally, the computational complexity of the proposed method and real running time with a detailed description of the running environment are laid out. The size of the image is $M \times N$, and the ring structuring element size is $m \times n$. For the proposed method, the computational complexity is mainly determined by the dilate operation. The dilate operation can be seen as a convolution operation essentially. According to Winograd algorithm [28], the dilate operation is computed in $O((M+m-1) \times (N+n-1))$ time. While the computational complexity of the traditional fastest algorithm TopHat is $O((M+m-1) \times (N+n-1) \times 2)$. In fact, morphological operations (dilation and erosion) as the basic image processing algorithms. All platforms, such as OpenCV, MATLAB, and high-level synthesis (HLS), have corresponding functions. Hence, our algorithm is extremely easy to achieve.

In comparison to the computational time consumption of the methods, we use some infrared images with the size 640×512. The average computational time consumption of different methods is offered in Table II. All experiments are implemented in MATLAB 2017a on a PC with a 2.4-GHz Intel i5 CPU and 16.0-GB memory. For the computational time consumption, GCM has brilliant performance, only 0.012 s, with

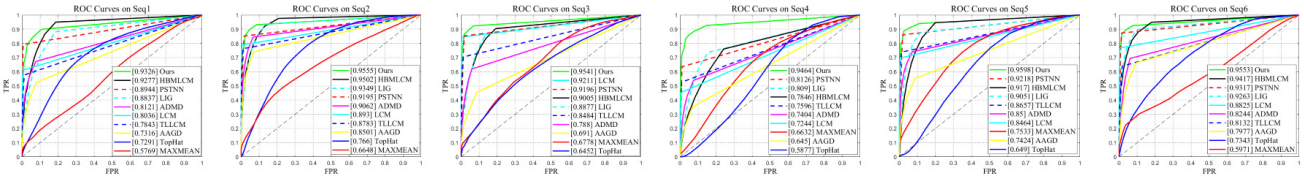

Fig. 3. ROC curves obtained by different methods on sequences 1–6.

a speed of at least two times faster than the baseline methods. Consequently, our method can enhance target availably in the complicit background with extreme efficiency.

IV. Conclusion

This letter has offered a fast and robust method based on GCM to detect small infrared targets against the diverse intricate background. The key idea of the proposed method is to use the dilate operation with a ring structuring element to exchange the gray value of the target and background, then utilize the ratio form and the difference form to enhance the target and suppress the background. The experimental result confirms that our method not only significantly increases the signal-to-clutter ratio (SCR) and BSF values, but also achieves a high-accuracy level and low false alarm rate. It is noteworthy that the computational time consumption of our method is extremely low, with only 0.012 s, which demonstrates that the detection speed of the proposed method is superior to other state-of-the-art methods. Consequently, the proposed method is quite suitable for real-time applications in single-frame small infrared target detection.

References

[1] X. Yang, Y. Zhou, D. Zhou, R. Yang, and Y. Hu, "A new infrared small and dim target detection algorithm based on multi-directional composite window," *Infr. Phys. Technol.*, vol. 71, pp. 402–407, Jul. 2015.

[2] V. T. Tom, T. Peli, M. Leung, and J. E. Bondaryk, "Morphology-based algorithm for point target detection in infrared backgrounds," *Proc. SPIE*, vol. 1954, pp. 2–11, May 1993.

[3] S. D. Deshpande, M. H. Er, V. Ronda, and P. Chan, "Max-mean and max-median filters for detection of small-targets," *Proc. SPIE*, vol. 3809, pp. 74–83, Oct. 1999.

[4] C. Q. Gao, D. Meng, Y. Yang, Y. Wang, X. Zhou, and A. G. Hauptmann, "Infrared patch-image model for small target detection in a single image," *IEEE Trans. Image Process.*, vol. 22, no. 12, pp. 4996–5009, Dec. 2013.

[5] L. Zhang and Z. Peng, "Infrared small target detection based on partial sum of the tensor nuclear norm," *Remote Sens.*, vol. 11, no. 4, p. 382, Feb. 2019.

[6] S. Aghaziyarati, S. Moradi, and H. Talebi, "Small infrared target detection using absolute average difference weighted by cumulative directional derivatives," *Infr. Phys. Technol.*, vol. 101, pp. 78–87, Sep. 2019.

[7] S. Moradi, P. Moallem, and M. F. Sabahi, "Fast and robust small infrared target detection using absolute directional mean difference algorithm," *Signal Process.*, vol. 177, Dec. 2020, Art. no. 107727.

[8] H. Zhang, L. Zhang, D. Yuan, and H. Chen, "Infrared small target detection based on local intensity and gradient properties," *Infr. Phys. Technol.*, vol. 89, pp. 88–96, Mar. 2018.

[9] C. Kwan and B. Budavari, "A high-performance approach to detecting small targets in long-range low-quality infrared videos," *Signal, Image Video Process.*, vol. 16, no. 1, pp. 93–101, Feb. 2022.

[10] H. Wang, Z. Zhao, C. Kwan, G. Zhou, and Y. Chen, "New results on small and dim infrared target detection," *Sensors*, vol. 21, no. 22, p. 7746, Nov. 2021.

[11] Y. Chen, G. Zhang, Y. Ma, J. U. Kang, and C. Kwan, "Small infrared target detection based on fast adaptive masking and scaling with iterative segmentation," *IEEE Geosci. Remote Sens. Lett.*, vol. 19, pp. 1–5, 2022.

[12] C. L. P. Chen, H. Li, Y. Wei, T. Xia, and Y. Y. Tang, "A local contrast method for small infrared target detection," *IEEE Trans. Geosci. Remote Sens.*, vol. 52, no. 1, pp. 574–581, Jan. 2014.

[13] Y. Wei, X. You, and H. Li, "Multiscale patch-based contrast measure for small infrared target detection," *Pattern Recognit.*, vol. 58, pp. 216–226, Oct. 2016.

[14] J. Han, Y. Yu, K. Liang, and H. Zhang, "Infrared small-target detection under complex background based on subblock-level ratio-difference joint local contrast measure," *Opt. Eng.*, vol. 57, no. 10, Oct. 2018, Art. no. 103105.

[15] L. Wu, Y. Ma, F. Fan, M. Wu, and J. Huang, "A double-neighborhood gradient method for infrared small target detection," *IEEE Geosci. Remote Sens. Lett.*, vol. 18, no. 8, pp. 1476–1480, Aug. 2021.

[16] J. Nie, S. Qu, Y. Wei, L. Zhang, and L. Deng, "An infrared small target detection method based on multiscale local homogeneity measure," *Infr. Phys. Technol.*, vol. 90, pp. 186–194, May 2018.

[17] Y. Shi, Y. Wei, H. Yao, D. Pan, and G. Xiao, "High-boost-based multiscale local contrast measure for infrared small target detection," *IEEE Geosci. Remote Sens. Lett.*, vol. 15, no. 1, pp. 33–37, Jan. 2018.

[18] J. Han, S. Moradi, I. Faramarzi, C. Liu, H. Zhang, and Q. Zhao, "A local contrast method for infrared small-target detection utilizing a tri-layer window," *IEEE Geosci. Remote Sens. Lett.*, vol. 17, no. 10, pp. 1822–1826, Oct. 2020.

[19] S. D. Pan et al., "Infrared small target detection based on double-layer local contrast measure," *Acta Photonica Sinica*, vol. 49, no. 1, pp. 184–192, 2020.

[20] Z. Cui, J. Yang, S. Jiang, J. Li, L. Lin, and Y. Gu, "An infrared-small-target detection method in compressed sensing domain based on local segment contrast measure," *Infr. Phys. Technol.*, vol. 93, pp. 41–52, Sep. 2018.

[21] J. Han, S. Liu, G. Qin, Q. Zhao, H. Zhang, and N. Li, "A local contrast method combined with adaptive background estimation for infrared small target detection," *IEEE Geosci. Remote Sens. Lett.*, vol. 16, no. 9, pp. 1442–1446, Sep. 2019.

[22] C. Xia, X. Li, L. Zhao, and R. Shu, "Infrared small target detection based on multiscale local contrast measure using local energy factor," *IEEE Geosci. Remote Sens. Lett.*, vol. 17, no. 1, pp. 157–161, Jan. 2020.

[23] X. Bai, "New class of top-hat transformation to enhance infrared small targets," *J. Electron. Imag.*, vol. 17, no. 3, Jul. 2008, Art. no. 030501.

[24] X. Bai and F. Zhou, "Analysis of new top-hat transformation and the application for infrared dim small target detection," *Pattern Recognit.*, vol. 43, no. 6, pp. 2145–2156, 2010.

[25] X. Sun et al., "A dataset for small infrared moving target detection under clutter background," *Chin. Sci. Data*, vol. 5, no. 6, p. 8, 2021.

[26] B. Hui et al., "A dataset for infrared detection and tracking of dim-small aircraft targets under-ground/air background," *China Sci. Data*, vol. 5, no. 3, pp. 291–302, 2020.

[27] L. Xu, Y. Wei, H. Zhang, and S. Shang, "Robust and fast infrared small target detection based on Pareto frontier optimization," *Infr. Phys. Technol.*, vol. 123, Jun. 2022, Art. no. 104192.

[28] A. Lavin and S. Gray, "Fast algorithms for convolutional neural networks," in *Proc. IEEE Conf. Comput. Vis. Pattern Recognit. (CVPR)*, Jun. 2016, pp. 4013–4021.